

# Constraints on neutron star radii based on chiral effective field theory interactions

K. Hebeler,<sup>1,\*</sup> J. M. Lattimer,<sup>2,†</sup> C. J. Pethick,<sup>3,4,‡</sup> and A. Schwenk<sup>5,6,1,§</sup>

<sup>1</sup>*TRIUMF, 4004 Wesbrook Mall, Vancouver, BC, V6T 2A3, Canada*

<sup>2</sup>*Department of Physics and Astronomy, Stony Brook University, Stony Brook, NY 11794-3800, USA*

<sup>3</sup>*The Niels Bohr Institute, Blegdamsvej 17, DK-2100 Copenhagen Ø, Denmark*

<sup>4</sup>*NORDITA, Roslagstullsbacken 21, SE-10691 Stockholm, Sweden*

<sup>5</sup>*ExtreMe Matter Institute EMMI, GSI Helmholtzzentrum für Schwerionenforschung GmbH, 64291 Darmstadt, Germany*

<sup>6</sup>*Institut für Kernphysik, Technische Universität Darmstadt, 64289 Darmstadt, Germany*

We show that microscopic calculations based on chiral effective field theory interactions constrain the properties of neutron-rich matter below nuclear densities to a much higher degree than is reflected in commonly used equations of state. Combined with observed neutron star masses, our results lead to a radius  $R = 9.7 - 13.9$  km for a  $1.4 M_\odot$  star, where the theoretical range is due, in about equal amounts, to uncertainties in many-body forces and to the extrapolation to high densities.

PACS numbers: 26.60.Kp, 97.60.Jd, 21.65.Cd

*Introduction.*— With the advances in observational capabilities, it is becoming possible to obtain direct evidence for the size of neutron stars [1]. Sources of information include measurements of optical radiation from nearby isolated neutron stars whose distances are known from parallax determinations, and observations of thermonuclear flares on the surfaces of neutron stars [2, 3]. Neutron star seismology [4], pulse profiles in X-ray pulsars [5] and moment of inertia measurements [6] are additional sources. In the near future, one further expects gravitational wave signals from collapsing stars and merging binary neutron stars to provide information about the equation of state of dense matter [7].

In nuclear physics, recent developments of effective field theory (EFT) and the renormalization group (RG) for nuclear forces enable controlled calculations of matter at nuclear densities [8–10]. In this framework, it is possible to estimate the theoretical uncertainties due to neglected many-body forces and from an incomplete many-body calculation. In this Letter, we show that such calculations of the equation of state (EOS) below nuclear densities constrain the properties of dense matter, and the radii of typical neutron stars, to a much higher degree than is reflected in current neutron star modeling.

*Neutron matter below nuclear densities.*— Our studies are based on microscopic calculations of neutron matter using chiral low-momentum two-nucleon (NN) and three-nucleon (3N) interactions [11]. The largest uncertainty for the neutron matter energy arises from the couplings  $c_3$  and (to a smaller extent)  $c_1$  that determine the leading two-pion-exchange three-body forces among neutrons in chiral EFT. We improve the range of  $c_3$  compared to Ref. [11] by taking  $c_3$  values from extractions based on the same couplings in the subleading two-pion-exchange NN interaction,  $c_3 = -(3.2 - 4.8) \text{ GeV}^{-1}$  [12–14]. In addition, we include a shift  $\delta c_3 = 1.0 \text{ GeV}^{-1}$  to take into account contributions at the next order for 3N forces [8]. In the following we therefore use  $c_3 = -(2.2 - 4.8) \text{ GeV}^{-1}$

and  $c_1 = -(0.7 - 1.4) \text{ GeV}^{-1}$  with a smooth  $n_{\text{exp}}^{3\text{N}} = 4$  regulator. The neutron matter calculations details are as in Ref. [11], which suggested that the energy is perturbative at nuclear densities. Using only NN interactions, we obtain a neutron matter energy per particle  $E_n^{\text{NN}}(\rho_0)/N = 10.4 \text{ MeV}$  at saturation density  $\rho_0 = 2.7 \times 10^{14} \text{ g cm}^{-3}$ . (We define the density  $\rho$  as the nucleon mass times the baryon density.) The inclusion of 3N forces leads to  $E_n(\rho_0)/N = 16.3 \pm 2.2 \text{ MeV}$ , dominated by the repulsive  $c_3$  contribution and the associated uncertainty. The 3N contribution of  $\approx 6 \text{ MeV}$  is to be compared to the NN potential energy  $\approx -26 \text{ MeV}$  (the kinetic energy is  $3/5 \varepsilon_{\text{F}}(\rho_0) \approx 36 \text{ MeV}$ ), and also the 3N uncertainty of  $\approx 2 \text{ MeV}$  is consistent with the contributions of higher-order 3N forces (given an approximate expansion parameter in chiral EFT of  $\sim 1/3$  at these momenta). Other microscopic calculations lie within our theoretical uncertainties [11], and at low densities  $\rho \sim \rho_0/10$ , the results are also consistent with calculations for resonant Fermi gases including effective range contributions [15].

*Neutron star matter.*— We extend our results to matter in beta equilibrium using the parametrization:

$$\frac{E(\rho, x)}{A} = \frac{E_n(\rho)}{N} - 4x(1-x)S_2(\rho) + \frac{3x\hbar c}{4} (3\pi^2 x\rho/m)^{1/3}, \quad (1)$$

where  $E_n(\rho)/N$  is given by our neutron matter results,  $m$  is the nucleon mass, and  $x$  the proton fraction. The last terms in Eq. (1) incorporate the contributions from protons through the symmetry energy  $S_2(\rho)$  and from electrons [16]. The proton fraction in beta equilibrium is given approximately by  $x(\rho) \approx [4S_2(\rho)/(\hbar c)]^3/(3\pi^2 \rho/m)$ , and for  $S_2(\rho_0) \approx 30 \text{ MeV}$ ,  $x(\rho_0) \approx 5\%$ . The energy difference between neutron matter and matter in beta equilibrium is  $-1.1 \text{ MeV}$ , and this will have only a minor impact on our final results. We extract  $S_2(\rho)$  for nuclear densities using empirical saturation properties,

$$S_2(\rho) = \frac{E_n(\rho)}{N} + a_V - \frac{K}{18\rho_0^2} (\rho - \rho_0)^2, \quad (2)$$

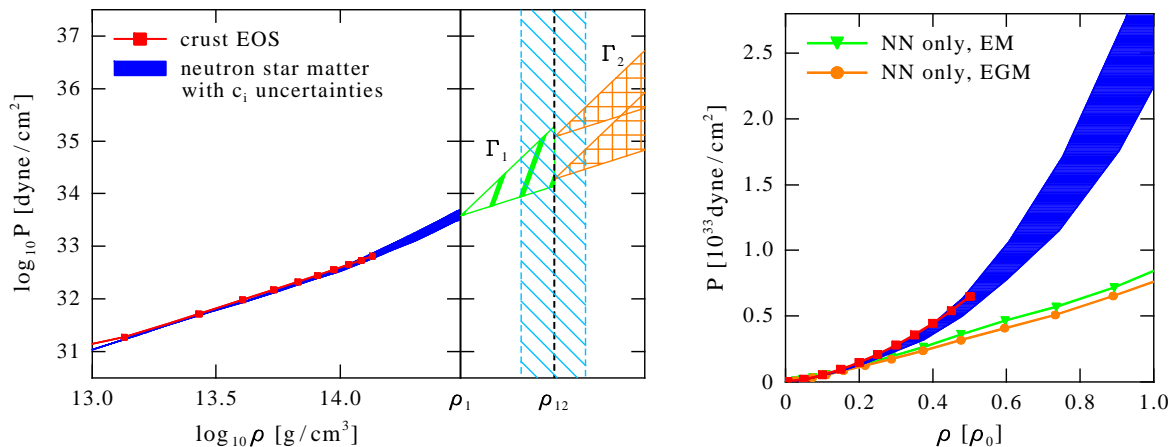


FIG. 1: Pressure of neutron star matter based on chiral low-momentum interactions for densities  $\rho < \rho_1$  (corresponding to a neutron density  $\rho_{1,n} = 1.1\rho_0$ ). The band estimates the theoretical uncertainties from many-body forces and from an incomplete many-body calculation. At low densities, the results are compared to a standard crust EOS [17], where the right panel demonstrates the importance of 3N forces. The extension to higher densities using piecewise polytropes (as explained in the text) is illustrated schematically in the left panel.

with binding energy  $a_V = 16$  MeV and incompressibility  $K = 230$  MeV (which are within theoretical uncertainties of the nuclear matter calculations of Ref. [10]). To include the symmetry energy in Eq. (1), we use the Ansatz  $S_2(\rho) = \bar{S}_2(\rho/\rho_0)^\gamma$  and fit  $\bar{S}_2 \equiv S_2(\rho_0)$  and  $\gamma$  to our neutron matter results. The fit has a relative uncertainty of  $< 5\%$  for densities  $\rho_0/8 < \rho < \rho_1 = 3.0 \times 10^{14} \text{ g cm}^{-3}$  ( $\rho_1$  corresponds to a neutron density  $\rho_{1,n} = 1.1\rho_0$ ). We obtain the following symmetry energy parameters and proton fractions:

$c_1$ [GeV $^{-1}$ ]	$c_3$ [GeV $^{-1}$ ]	$\bar{S}_2$ [MeV]	$\gamma$	$x(\rho_0)$
-0.7	-2.2	30.1	0.5	4.8%
-1.4	-4.8	34.4	0.6	7.2%
NN-only EM		26.5	0.4	3.3%
NN-only EGM		25.6	0.4	2.9%

The resulting pressure of neutron star matter is shown in Fig. 1 for densities  $\rho < \rho_1$ , where the band is dominated by the uncertainty in  $c_3$ . The comparison of these parameter-free calculations to a standard crust EOS [17] shows good agreement to low densities  $\rho \gtrsim \rho_0/10$  within the theoretical uncertainties. In addition, the right panel of Fig. 1 demonstrates the importance of 3N forces. The pressure obtained from low-momentum NN interactions only, based on the RG-evolved  $N^3\text{LO}$  potentials of Entem and Machleidt (EM) [12] or Epelbaum *et al.* (EGM) [13], differ significantly from the crust EOS at  $\rho_0/2$ .

*Neutron stars.*— The structure of non-rotating neutron stars without magnetic fields is determined by solving the Tolman-Oppenheimer-Volkov (TOV) equations. Because the central densities reach values higher than  $\rho_1$ , we need to extend the uncertainty band for the pressure of neutron star matter beyond  $\rho_1$ . To this end, we introduce a transition density  $\rho_{12}$  that separates two higher-density regions, and describe the pressure by piecewise polytropes,  $P(\rho) = \kappa_1 \rho^{\Gamma_1}$  for  $\rho_1 < \rho < \rho_{12}$ , and

$P(\rho) = \kappa_2 \rho^{\Gamma_2}$  for  $\rho > \rho_{12}$ , where  $\kappa_{1,2}$  are determined by continuity of the pressure. Ref. [18] has shown that such an EOS with  $1.5 < \Gamma_{1,2} < 4.0$  and transition densities  $\rho_{12} \approx (2.0 - 3.5)\rho_0$  can mimic a large set of neutron star matter EOS. We therefore extend the pressure of neutron star matter based on chiral EFT in this way, with  $1.5 < \Gamma_{1,2} < 4.5$  and  $1.5 < \rho_{12}/\rho_0 < 4.5$ , as illustrated in Fig. 1. The possibility of a phase transition at higher densities is implicitly taken into account if one regards the  $\Gamma_{1,2}$  values as averages over some density range.

We solve the TOV equations for the limits of the pressure band below nuclear densities continued to higher densities by the piecewise polytropes. The range of  $\Gamma_{1,2}$  and  $\rho_{12}$  can be constrained further, first, by causality, which limits the sound speed to the speed of light and, second, by the requirement that the EOS support a  $1.65M_\odot$  star [19]. The resulting allowed range of polytropes is shown by the light blue band at higher density in Fig. 2 [27]. The comparison with a representative set of EOS used in the literature [16] demonstrates that the pressure based on chiral EFT interactions (the darker blue band) sets the scale for the allowed higher-density extensions and is therefore extremely important. It also significantly reduces the spread of the pressure at nuclear densities from a factor 6 at  $\rho_1$  in current neutron star modeling to a factor 1.5.

*Results.*— In Fig. 3 we show the neutron star  $M$ - $R$  curves obtained from the allowed EOS range. The blue region corresponds to the blue band for the pressure in Figs. 1 and 2. At the limits of this region, the pressure of neutron star matter is continued as piecewise polytropes, and all curves end when causality is violated. Should causality be violated before the maximum mass (at  $dM/dR = 0$ ) is reached, one could continue the  $M$ - $R$  curves by enforcing causality. This would lead to a somewhat larger maximum mass, but would not affect

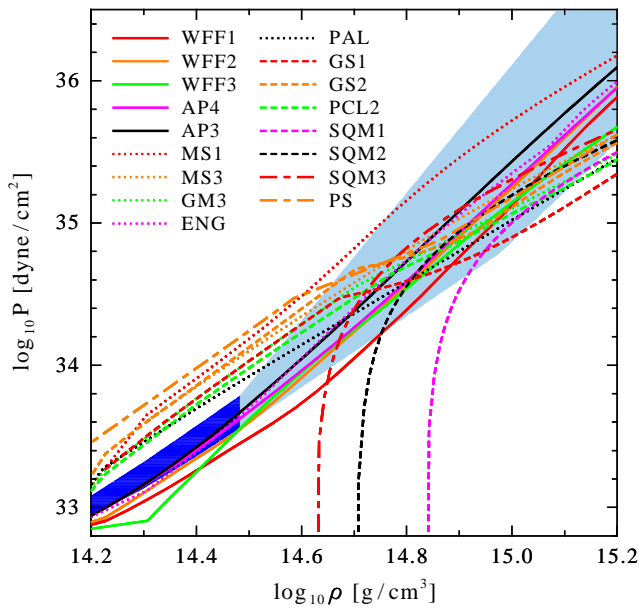


FIG. 2: Comparison of the EOS based on Fig. 1 to a representative set of EOS used in the literature [16]. The blue band corresponds to the band in Fig. 1 and the lighter region covers the range of polytropes allowed (see text for discussion).

the masses and radii of neutron stars with lower central densities. We observe from the transition density points  $\rho_{12}$  in Fig. 3 that the range of  $\Gamma_1$  dominates the uncertainty of the general extension to high densities. Smaller values of  $\Gamma_1$  are excluded because the associated EOS is not able to support a  $1.65M_\odot$  star. The larger allowed values of the polytropic indices lead to very low central densities  $\rho \sim (2.0 - 2.5)\rho_0$ .

We find that the pressure at nuclear densities and below sets the scale for the  $M-R$  results. The blue region in Fig. 3 ends almost at the central value of the radius results. For a  $1.4M_\odot$  star, the radius is constrained to  $R = 9.3 - 13.5$  km, as indicated by the vertical band. While going from neutron matter to beta equilibrium can reduce individual results for an  $1.4M_\odot$  star by up to 0.4 km, the overall result is very similar for pure neutron matter with  $R = 9.3 - 13.3$  km. Furthermore, if a  $2.0M_\odot$  star were to be observed, this would reduce the allowed range to  $R = 10.5 - 13.3$  km. As for the EOS in Fig. 2, the presented radius constraint significantly reduces the spread of viable neutron star models, *e.g.*, it is difficult to see how one can obtain  $R \approx 15$  km as is the case for the Shen EOS [20]. Finally, our results are more rigorous than an estimate based on the empirical  $PR^{-4}$  correlation [16], which for the values of the pressure we find,  $P(\rho_0) = 1.4 - 2.1 \text{ MeV fm}^{-3}$ , implies  $R = 9.4 - 11.9$  km.

When chiral 3N forces are neglected, the neutron star radius is significantly smaller, with  $R^{\text{NN}} = 8.8 - 11.0$  km as shown in Fig. 4 based on low-momentum NN interactions only. This demonstrates that the theoretical error for the radius of a  $1.4M_\odot$  star is due, in about equal

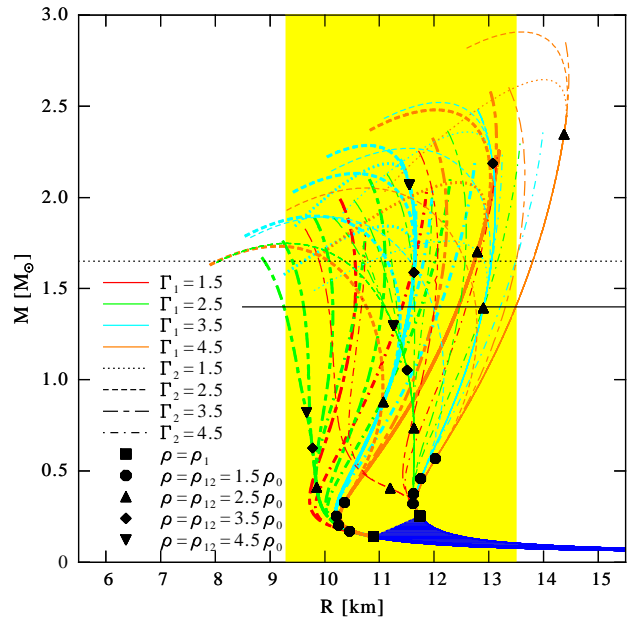


FIG. 3: Neutron star  $M-R$  results for the EOS based on Fig. 1. The thick (thin) lines, corresponding to the left (right) branch, start from the low pressure limit  $c_1 = -0.7 \text{ GeV}^{-1}$ ,  $c_3 = -2.2 \text{ GeV}^{-1}$  (high pressure limit  $c_1 = -1.4 \text{ GeV}^{-1}$ ,  $c_3 = -4.8 \text{ GeV}^{-1}$ ). The blue region corresponds to the band below nuclear densities in Figs. 1 and 2. The different piecewise polytropes can be identified from the colors/lines indicating  $\Gamma_1/\Gamma_2$  and from the points denoting  $\rho_{12}$ . The vertical band gives the radius constraint for a  $1.4M_\odot$  star.

amounts, to the uncertainties in 3N forces and to the extension to higher densities dominated by  $\Gamma_1$ .

*Effect of the crust.*— In our calculations, the difference between the neutron and proton masses was neglected and the phases were assumed to be spatially uniform. In this approximation, matter at low density consists only of neutrons. The impact of using a more realistic EOS at low densities can be investigated by observing that the surface gravity of the star is approximately constant in the outer layers. By integrating the equation of hydrostatic equilibrium from the surface of the star up to a crust density  $\rho_c$ , one finds that the mass between the density  $\rho_c$  and the surface is proportional to the pressure at  $\rho_c$  [21]. Thus the stellar mass is to a good approximation unaffected by changes in the EOS at  $\rho < \rho_c$ . To determine how changes in the low-density EOS affect the radius, we note that the thickness of the crust ( $\rho < \rho_c$ ) is  $\Delta R = [\mu(\rho_c) - \mu_s]/[mg(1+z)]$ , where  $g = GM(1+z)/R^2$  is the surface gravity, with surface redshift  $1+z = [1 - 2GM/(Rc^2)]^{-1/2}$  [22]. Here  $\mu_s$  is the (neutron) chemical potential at the surface of the star, where the pressure is zero. For the calculations in this paper,  $\mu_s = mc^2$ , while for realistic EOS of cold catalysed matter it includes the binding energy per particle of solid iron,  $\approx 8 \text{ MeV}$ . Thus use of a more realistic EOS at low densities will increase the radius of the star

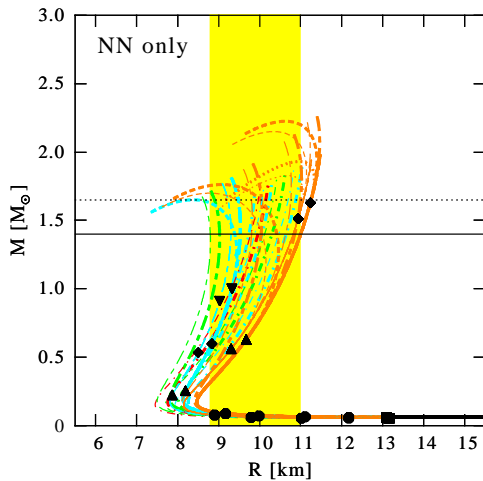


FIG. 4: Same as Fig. 3 but for NN-only interactions (thick lines are based on EM [12] and thin lines on EGM [13]).

by  $8 \text{ MeV}/[mg(1+z)]$ . This increases the radius for a  $1.4M_{\odot}$  star by  $0.2 - 0.5 \text{ km}$ , leading to our final result  $R = 9.7 - 13.9 \text{ km}$ .

*Other implications.*— The relatively weak density dependence of the nuclear symmetry energy also makes predictions for the neutron skin of  $^{208}\text{Pb}$ . The symmetry energy of a nucleus in the liquid droplet model consists largely of bulk and surface contributions, the latter being determined by an integration of  $S_2(\rho)$  through the nucleus [23]. Assuming a quadratic density dependence for the energy of symmetric nuclear matter and our results for  $S_2 = \bar{S}_2(\rho/\rho_0)^\gamma$ , one finds the ratio of the surface and bulk symmetry parameters to be  $S_s/\bar{S}_2 \approx 1.85 \pm 0.25$ . This leads to a neutron skin thickness  $\delta R = 0.16 - 0.2 \text{ fm}$  for  $^{208}\text{Pb}$ , while the correlation with the slope of the neutron matter energy [24] gives  $0.14 - 0.19 \text{ fm}$ . Therefore we predict  $\delta R = 0.14 - 0.2 \text{ fm}$ , which can be tested in the parity-violating electron scattering experiment (PREX) [25]. Finally, we note that in a complementary approach [26], the EOS of high-density matter is constrained from perturbative QCD calculations, and that our results are very consistent with the astrophysical estimates of Ref. [3].

In this Letter, we have demonstrated that microscopic calculations based on chiral EFT and many-body theory constrain the pressure of matter at nuclear densities to within  $\pm 25\%$ . This should be taken into account in modeling stellar collapse, black hole formation, and neutron stars. Even allowing for uncertainties in the low-energy theory and the extrapolation to higher densities, we find that the radius of a neutron star depends only weakly on its mass and for a  $1.4M_{\odot}$  star is rather well constrained.

This paper was initiated at the MICRA2009 Workshop in Copenhagen, funded in part by the ESF AstroSim and CompStar networks. We thank the Niels Bohr International Academy for the kind hospitality. This work was supported in part by NSERC, the U.S. DOE

grant DE-AC02-87ER40317 and by the Helmholtz Alliance Program of the Helmholtz Association, contract HA216/EMMI “Extremes of Density and Temperature: Cosmic Matter in the Laboratory”. TRIUMF receives funding via a contribution through the NRC Canada.

\* E-mail: hebeler@triumf.ca

† E-mail: lattimer@astro.sunysb.edu

‡ E-mail: pethick@nbi.dk

§ E-mail: schwenk@physik.tu-darmstadt.de

- [1] J. M. Lattimer and M. Prakash, Phys. Rept. **442**, 109 (2007).
- [2] F. Özel, G. Baym and T. Güver, arXiv:1002.3153.
- [3] A. W. Steiner, J. M. Lattimer and E. F. Brown, arXiv:1005.0811.
- [4] L. Samuelsson and N. Andersson, MNRAS **374**, 256 (2007); A. W. Steiner and A. L. Watts, Phys. Rev. Lett. **103**, 181101 (2009).
- [5] D. A. Leahy *et al.*, Astrophys. J. **691**, 1235 (2009).
- [6] J. M. Lattimer and B. F. Schutz, Astrophys. J. **629**, 979 (2005).
- [7] V. Ferrari, L. Gualtieri and F. Pannarale, Phys. Rev. D **81**, 064026 (2010).
- [8] E. Epelbaum, H.-W. Hammer and U.-G. Meißner, Rev. Mod. Phys. **81**, 1773 (2009).
- [9] S. K. Bogner, R. J. Furnstahl and A. Schwenk, Prog. Part. Nucl. Phys. **65**, 94 (2010).
- [10] S. K. Bogner *et al.*, Nucl. Phys. A **763**, 59 (2005); and arXiv:0903.3366.
- [11] K. Hebeler and A. Schwenk, Phys. Rev. C **82**, 014314 (2010).
- [12] D. R. Entem and R. Machleidt, Phys. Rev. C **68**, 041001(R) (2003).
- [13] E. Epelbaum, W. Glöckle and U.-G. Meißner, Nucl. Phys. A **747**, 362 (2005).
- [14] M. C. M. Rentmeester, R. G. E. Timmermans and J. J. de Swart, Phys. Rev. C **67**, 044001 (2003).
- [15] A. Schwenk and C. J. Pethick, Phys. Rev. Lett. **95**, 160401 (2005); A. Gezerlis and J. Carlson, Phys. Rev. C **77**, 032801 (2008).
- [16] J. M. Lattimer and M. Prakash, Astrophys. J. **550**, 426 (2001).
- [17] G. Baym, C. J. Pethick and P. Sutherland, Astrophys. J. **170**, 299 (1971); J. W. Negele and D. Vautherin, Nucl. Phys. A **207**, 298 (1973).
- [18] J. S. Read *et al.*, Phys. Rev. D **79**, 124032 (2009).
- [19] P. C. C. Freire *et al.*, arXiv:0907.3219.
- [20] H. Shen *et al.*, Nucl. Phys. A **637**, 435 (1998).
- [21] C. P. Lorenz, D. G. Ravenhall and C. J. Pethick, Phys. Rev. Lett. **70**, 379 (1993).
- [22] J. M. Lattimer *et al.*, Astrophys. J. **425**, 802L (1994).
- [23] A. W. Steiner *et al.*, Phys. Rept. **411**, 325 (2005).
- [24] B. A. Brown, Phys. Rev. Lett. **85**, 5296 (2000); S. Typel and B. A. Brown, Phys. Rev. C **64**, 027302 (2001).
- [25] R. Michaels, P. A. Souder and G. M. Urciuoli, Jefferson Laboratory Proposal, PR-00-003 (2003); C. J. Horowitz *et al.*, Phys. Rev. C **63**, 025502 (2001).
- [26] A. Kurkela *et al.*, arXiv:1006.4062.
- [27] We have maximized the range of  $\Gamma_1$  given the causality and  $1.65M_{\odot}$  star constraint